JACS
JOURNAL OF THE AMERICAN CHEMICAL SOCIETY

ARTICLE

pubs.acs.org/JACS

Near-Complete Suppression of Surface Recombination in Solar Photoelectrolysis by "Co-Pi" Catalyst-Modified W:$BiVO_4$

Diane K. Zhong, Sujung Choi, and Daniel R. Gamelin*

Department of Chemistry, University of Washington, Seattle, Washington 98195-1700, United States

Supporting Information

ABSTRACT: The influence of an earth-abundant water oxidation electrocatalyst (Co-Pi) on solar water oxidation by W:$BiVO_4$ has been studied using photoelectrochemical (PEC) techniques. Modification of W:$BiVO_4$ photoanode surfaces with Co-Pi has yielded a very large (~440 mV) cathodic shift in the onset potential for sustained PEC water oxidation at pH 8. PEC experiments with H_2O_2 as a surrogate substrate have revealed that interfacing Co-Pi with these W:$BiVO_4$ photoanodes almost completely eliminates losses due to surface electron−hole recombination. The results obtained for W:$BiVO_4$ are compared with those reported recently for Co-Pi/α-Fe_2O_3 photoanodes. The low absolute onset potential of ~310 mV vs RHE achieved with the Co-Pi/W:$BiVO_4$ combination is promising for overall solar water splitting in low-cost tandem PEC cells, and is encouraging for application of this surface modification strategy to other candidate photoanodes.

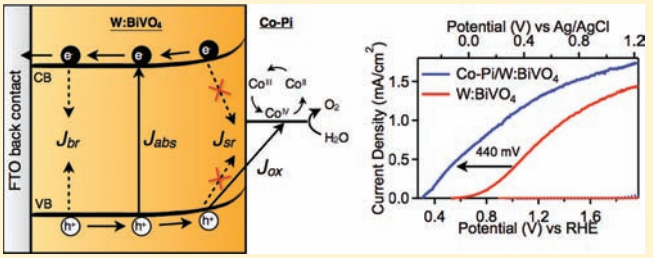

INTRODUCTION

Photoelectrochemical (PEC) water splitting is a promising strategy for the capture and storage of the Earth's abundant solar energy influx.[1−5] The greatest challenge in this chemistry is the water oxidation reaction, which is a multistep, four-electron, four-proton process. Because of kinetic barriers, large overpotentials are typically required to drive this reaction electrochemically. In PEC water splitting, additional overpotentials are needed to also overcome competing electron−hole recombination processes, at the expense of solar-energy-conversion efficiency.[2−5] In both experiments, these needs can be addressed in part by introduction of surface electrocatalysts, which improve water-oxidation kinetics and thereby improve energy conversion efficiencies. To a large extent, successful integration of water-oxidation catalysts with PEC photoanodes has been limited to Pt or RuO_2.[5]

Any potential PEC technology must balance efficiency against cost and scalability considerations. For this reason, much research has been focused on the development of oxides as photoelectrode materials.[2−8] Oxides are frequently inexpensive, stable, easily prepared on a large scale, and robust under PEC operating conditions. Successful development of even moderately efficient oxide PEC cells for solar water splitting would be a major advance toward the goal of large-scale, distributable solar hydrogen generation.

Among candidate oxides, $BiVO_4$ (bismuth yellow) has attracted broad attention recently as an inexpensive and robust semiconductor for potential application as a water-oxidation photocatalyst.[9−23] $BiVO_4$ exists in three polymorphs, with the monoclinic scheelite structure being the most reactive for water oxidation.[10,17] With its direct band gap of ~2.4−2.5 eV at room temperature, scheelite $BiVO_4$ can use visible light to drive water oxidation. PEC measurements using polycrystalline photoanodes show that $BiVO_4$ has a relatively low onset potential for water oxidation (~0.5 V vs RHE) and can achieve photocurrent densities of a few mA/cm^2 with visible-light excitation.[11] Doping,[12,15,18] along with surface catalyst modification,[19,20,24] may improve the overall PEC water-oxidation efficiencies of $BiVO_4$ photoanodes. For example, several studies have demonstrated improvement of $BiVO_4$ PEC performance by tungsten doping.[15,18,22] According to density functional theory calculations, tungsten is an n-type dopant in $BiVO_4$, substituting for V^{5+} as W^{6+} ($+e^-_{CB}$).[23] Mott−Schottky plots confirm that tungsten doping increases the majority carrier density in $BiVO_4$.[15,18]

In the present study, we evaluate the effects of interfacing W:$BiVO_4$ photoanodes with cobalt-phosphate ("Co-Pi"), a simple but effective earth-abundant water-oxidation electrocatalyst.[25−27] Although many surface catalysts have already been explored with $BiVO_4$ and related photoanodes,[22] Co-Pi offers the attractive advantages of being easily integrated with complex surface topologies, in addition to being regenerative under PEC conditions. Co-Pi has previously been shown to improve PEC water oxidation by various photoelectrodes including α-Fe_2O_3,[28−31] ZnO,[32] WO_3,[33] Si/Co,[34] and Si/ITO.[34,35] While the present work was in progress, encouraging data were reported showing phenomenologically that Co-Pi also markedly improves the PEC performance of W:$BiVO_4$,[22] although analysis of this observation was not the focus of that study. In all cases, Co-Pi deposition onto the photoanode surface yielded large cathodic shifts of the onset potentials for water oxidation. The thickness of the Co-Pi layer

Received: August 4, 2011
Published: September 26, 2011

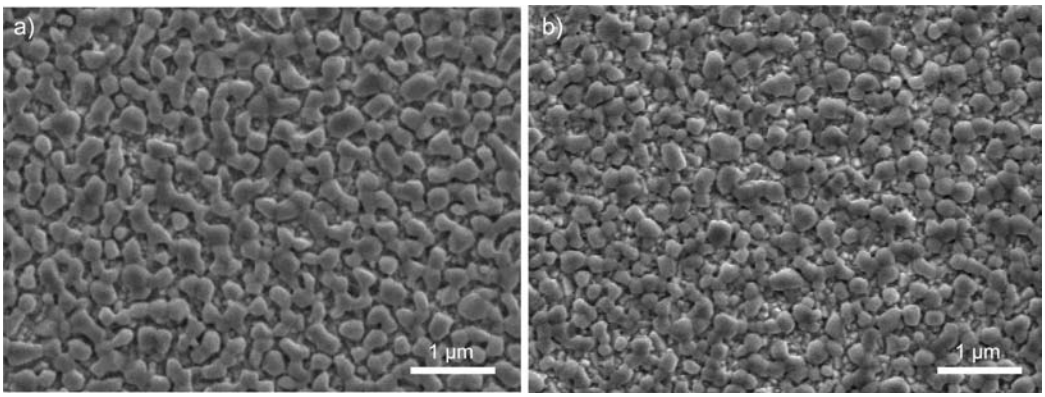

Figure 1. Top-view SEM images of representative (a) $BiVO_4$ and (b) W:$BiVO_4$ photoanodes. Both films were estimated from cross-sectional SEM to be ~300 nm.

was shown to play an important role in photoanode performance, with increased Co-Pi thicknesses reducing overpotentials but also impairing the ability to sustain high current densities.[29] This trend has been attributed to competition between productive water oxidation and unproductive surface electron−hole recombination,[29,30] highlighting a key contrast between electrochemical and PEC water oxidation. In electrochemical water oxidation with Co-Pi, thicker catalyst layers improve overall electrolysis current densities.[27] In PEC water oxidation with Co-Pi, thick catalyst layers reduce the ability of productive water oxidation to compete with nonproductive surface electron−hole recombination.[29,30] To circumvent this kinetic bottleneck, a photoassisted electrodeposition method was developed to deposit thin (<30 nm), uniform, and conformal Co-Pi layers onto mesostructured photoelectrode surfaces.[30]

Here, we report that photoassisted electrodeposition of Co-Pi onto W:$BiVO_4$ photoanodes results in a remarkable ~440 mV cathodic shift in the onset potential for sustained water oxidation, significantly larger than the cathodic shifts observed with other oxide photoanodes.[28−30,32,33] PEC water oxidation by the resulting Co-Pi/W:$BiVO_4$ composite photoelectrodes is shown to be as facile as PEC hydrogen peroxide oxidation by the parent photoelectrode (W:$BiVO_4$), indicating extremely effective hole capture and conversion to O_2 at the Co-Pi/W:$BiVO_4$ interface. Analysis shows nearly complete elimination of surface electron−hole recombination at all potentials following Co-Pi deposition, leading to nearly quantitative surface hole capture and onset potentials as low as 310 mV vs RHE. These results highlight the critical importance of suppressing surface electron−hole recombination in order to achieve efficient PEC solar water oxidation, and demonstrate the effective suppression of such losses in an attractive and widely investigated oxide photocatalyst, $BiVO_4$, using the simple, earth-abundant electrocatalyst, Co-Pi.

EXPERIMENTAL SECTION

$BiVO_4$ photoanodes were fabricated by modification of literature metal−organic decomposition (MOD) methods.[11,16] Equimolar amounts of bismuth nitrate hexahydrate (0.173 g) and vanadyl acetylacetonate (0.095 g) were added to a 5 mL solution of 1:8.25 acetic acid and acetylacetone. The dark green solution was then sonicated for 15 min. For W:$BiVO_4$ photoanodes, 7 atomic % tungstic acid was added to the solution and the vanadium concentration was decreased to 93%. The final solution was spin coated onto an FTO substrate (TEC 15, Hartford Glass Co.) at 1000 rpm for 30 s and annealed at 500 °C for 10 min for each of several coats. Altogether, 16 coats were applied, with a 2 h annealing time after 8 coats. The final films were annealed for 8 h at 500 °C.

PEC measurements were performed in a three-electrode PEC cell with the photoanode as the working electrode, Ag/AgCl as the reference electrode, and a Pt wire mesh as the counter electrode. A Gamry Series G 300 potentiostat was used for all measurements. Unless otherwise stated, all PEC measurements were conducted under 1 sun AM 1.5 simulated sunlight with an Oriel 96000 solar simulator integrating a 150 W xenon arc lamp and Oriel 81094 filter. The photoanodes were masked with a 6 mm aperture to maintain the same area for dark and light measurements. Experiments were performed in 0.1 M potassium phosphate (KPi) buffered to pH 8, unless otherwise stated. Potentials are reported as measured vs Ag/AgCl and as calculated vs RHE using the Nernstian relation $E_{RHE} = E_{Ag/AgCl} + 0.0591pH + 0.1976$ V. Transient photocurrent density measurements were performed under constant applied potential for 35 s with a 30 s light pulse turned on after 2 s. IPCE measurements were collected with a 250 W tungsten light source directed through an Oriel Cornerstone 74000 monochromator blazed at 350 nm. Light intensity was measured with a calibrated silicon detector with a maximum light output of ~6 mW/cm^2 at 540 nm. We have previously demonstrated[30] that integration of IPCE data from this system with the standard solar spectral distribution predicts solar photocurrents that agree well with the values measured under 1 sun AM1.5 irradiation, verifying the light source and confirming the solar photocurrent magnitudes reported.

Co-Pi was applied onto W:$BiVO_4$ photoanodes by the photoassisted electrodeposition method described previously.[30] Co-Pi was deposited for 3−5 min at ~0.2−0.4 V vs RHE, with typical photocurrent densities of ~1−4 μA/cm^2 during deposition. Oxygen detection was performed in a three-neck flask with an optical window by an Ocean Optics NeoFox fluorescence measurement system equipped with a temperature sensor and FOXY-AR-WW oxygen probe. The instrument was calibrated by a two-point calibration in air and under argon. The total oxygen evolved was calculated from the amount of oxygen measured in the headspace using the ideal gas law and the amount of oxygen dissolved in the electrolyte using Henry's law. The volume of the liquid and headspace were measured to be 97.5 and 82.5 mL, respectively. Prior to the measurement, the electrolyte, 0.1 M pH 8 KPi, was degassed and purged with argon. Measurements were conducted in argon in the same three-electrode configuration described for PEC experiments. The photoanode was not masked for the O_2 measurements, making the illumination power density approximate (~1 sun).

Scanning electron microscopy (SEM) and energy dispersive X-ray (EDX) analyses were conducted using an FEI Sirion scanning electron microscope equipped with an energy dispersive spectrometer at an accelerating voltage of 5 keV for images and 10 keV for EDX measurements.

X-ray diffraction (XRD) patterns were collected using a Bruker F8 Focus X-ray diffractometer and calibrated using a NIST standard reference corundum alumina disk as an external standard and FTO as an internal standard.

RESULTS

A. General Aspects of the $BiVO_4$ and W:$BiVO_4$ Photoanodes. Figure 1 shows SEM images of representative $BiVO_4$ and W:$BiVO_4$ photoanodes used for the PEC measurements described in the present study. The $BiVO_4$ photoanodes are polycrystalline with primary features having dimensions of ~100−200 nm. The structures seen in Figure 1a are similar to those reported for $BiVO_4$ made by the same technique previously.[11] Tungsten incorporation does not substantially alter the film morphology (Figure 1b), although slightly smaller feature sizes are observed. EDX mapping of bismuth, vanadium, and tungsten show uniform distribution of these elements throughout the W:$BiVO_4$ films (see the Supporting Information). The thicknesses of these films were both estimated from cross-sectional SEM to be ~300 nm.

X-ray diffraction from these $BiVO_4$ photoanodes (see the Supporting Information) agrees well with expectations for monoclinic scheelite.[10,36,37] Upon tungsten incorporation, small monoclinic WO_3 peaks were also observed, indicating that at least some of the tungsten has segregated out of the $BiVO_4$ lattice. Tungsten also appears to be doped into $BiVO_4$ based on the observed shifts of the diffraction peaks (see the Supporting Information). Tungsten (W^{6+}) likely substitutes for V^{5+},[15,23] causing lattice deformation.[36,37] To our knowledge, Vegard's law for W-doping of $BiVO_4$ has not been thoroughly documented, so the percentage W^{6+} incorporated within the $BiVO_4$ is unknown. Tungsten doping does not introduce any noticeable new electronic transitions (see the Supporting Information). Absorption features from phase-segregated WO_3 are also not evident, presumably because of the small amount present.

For our $BiVO_4$ photoanodes, photocurrent densities achieved with back-side illumination are greater than those achieved with front-side illumination (see the Supporting Information), indicating that hole diffusion is more facile than electron diffusion in these $BiVO_4$ films. Upon tungsten incorporation, the difference between photocurrents obtained with front- and back-side illumination decreases substantially, suggesting that electron mobility is improved by tungsten doping, consistent with W^{6+} ($+e^-_{CB}$) incorporation. Similarly, under front-side illumination, the IPCE of $BiVO_4$ drops rapidly at wavelengths below ~460 nm (see the Supporting Information), whereas the same film under back-side illumination shows its IPCE maximum at ~430 nm. Conversely, front-side illumination of W:$BiVO_4$ yields more photocurrent than back-side illumination and has its maximum at shorter wavelengths. These trends are again manifestations of the improved electron mobility of $BiVO_4$ following tungsten doping.

The above results are consistent with those reported previously for $BiVO_4$ and W:$BiVO_4$ photoanodes,[11,15,18,37] and hence, the conclusions drawn from investigation of these photoanodes are expected to be generally applicable to other $BiVO_4$-based photoanodes.

B. Co-Pi Deposition and Water Oxidation. We next examined modification of the W:$BiVO_4$ surfaces with the amorphous electrocatalyst Co-Pi, which excels at water oxidation. We have previously reported that photoassisted electrodeposition of

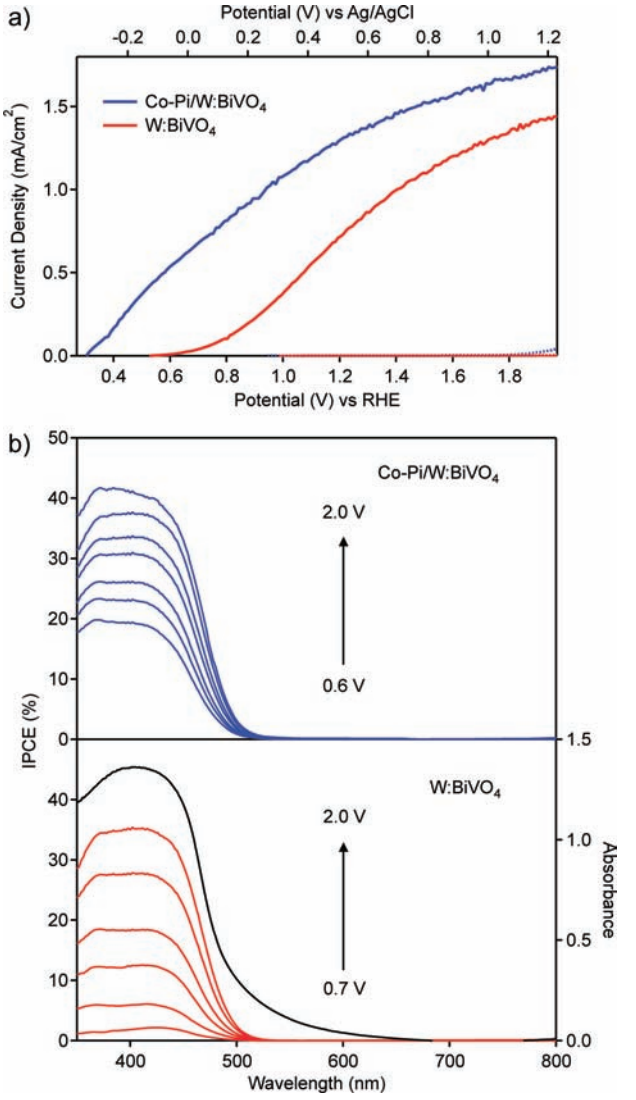

Figure 2. (a) Current density−voltage ($J-V$) curves measured for a W:$BiVO_4$ photoanode before (red) and after (blue) photoassisted electrodeposition of Co-Pi under front-side illumination (solid line) and in the dark (dotted line). Experiments were performed with 1 sun, AM 1.5 simulated solar irradiation in 0.1 M KPi buffer at pH 8 at a scan rate of 10 mV/s. (b) Absorption (black) and photocurrent action spectra of the same W:$BiVO_4$ photoanode before (red) and after (blue) Co-Pi deposition. Photocurrent action spectra were collected at applied potentials of 0.6, 0.7, 0.8, 1.0, 1.2, 1.6, and 2.0 V vs RHE.

Co-Pi onto α-Fe_2O_3 photoanodes yields superior PEC performance than Co-Pi electrodeposition or Co^{2+} surface impregnation.[30] In contrast with electrolysis, PEC water oxidation appears to be quite sensitive to the Co-Pi film thickness, slowing considerably at thicknesses exceeding only a few tens of nanometers.[29] Electrodeposition of Co-Pi onto α-Fe_2O_3 photoanodes yielded islands where pinholes exposed the more conductive TCO substrate, but photoassisted electrodeposition yielded uniform thin layers of Co-Pi, deposited only where light generated oxidizing equivalents, and this procedure was shown to translate into better PEC performance.[30] For these reasons, Co-Pi was deposited onto W:$BiVO_4$ by photoassisted electrodeposition in the present study. Similar to the behavior of α-Fe_2O_3,[29] deposition of excess Co-Pi onto $BiVO_4$ leads to a decrease in sustainable

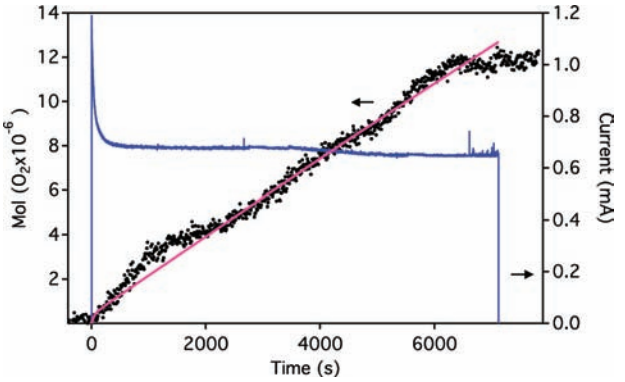

Figure 3. Total O_2 produced (black dots) from approximately 1 sun AM1.5 illumination of a Co-Pi/W:$BiVO_4$ photoanode poised at 1 V vs RHE in 0.1 M KPi buffered at pH 8. The pink curve shows the O_2 evolution calculated from the measured photocurrent (blue curve) assuming 100% faradaic efficiency.

PEC water oxidation rates for both front- and back-side illumination, so all measurements reported here were performed with front-side illumination following optimization of the Co-Pi thickness for PEC current density.

Figure 2 summarizes PEC results obtained from a representative W:$BiVO_4$ photoanode. Figure 2a shows $J-V$ curves collected using a W:$BiVO_4$ photoanode before and after Co-Pi deposition. Co-Pi deposition yields a remarkable ~440 mV cathodic shift in the onset potential for water oxidation relative to the parent W:$BiVO_4$ photoanode. As a result, the Co-Pi/W:$BiVO_4$ photoanode exhibits an onset potential of only ~310 mV vs RHE. This onset potential is ~550 mV lower than that obtained with the best Co-Pi/α-Fe_2O_3 photoanodes (~860 mV).[30] Very similar results are obtained using $BiVO_4$ except that the overall photocurrent densities are smaller (see the Supporting Information). The maximum photocurrent densities of these Co-Pi/W:$BiVO_4$ photoanodes are not as large as those achieved with Co-Pi/α-Fe_2O_3 photoanodes, but because of the very low onset potentials the overall thermodynamic solar-to-hydrogen conversion efficiencies of the single-junction PEC cells based on Co-Pi/W:$BiVO_4$ are greater (vide infra).

Photocurrent action spectra (Figure 2b) mirror the substantial improvements seen in Figure 2a after Co-Pi modification, especially at low applied potentials. Co-Pi itself does not contribute any additional features to the photocurrent action spectra of the composite Co-Pi/W:$BiVO_4$ photoanodes. Instead, increased IPCE values are observed across the entire W:$BiVO_4$ response curve. Co-Pi yields an IPCE maximum of ~20% at 0.6 V vs RHE (λ = 370 nm), where essentially no photocurrent was observed using W:$BiVO_4$ alone, and of ~33% at 1.23 V vs RHE. These data confirm the function of Co-Pi as a surface electrocatalyst that improves conversion of photogenerated holes into productive redox equivalents, without directly contributing to light harvesting or causing significant occlusion of the underlying photoanode.

Oxygen detection experiments confirm that this enhanced photocurrent is associated with O_2 evolution. Figure 3 plots O_2 generation vs time in a PEC experiment performed while irradiating a Co-Pi/W:$BiVO_4$ photoanode with 1 sun simulated AM1.5 light at 1 V vs RHE in 0.1 M KPi buffered at pH 8. At this bias, the parent W:$BiVO_4$ photoanode shows only one-third of the PEC current density of the Co-Pi/W:$BiVO_4$ photoanode. Following an initial spike when irradiation begins, attributable in part to cobalt oxidation, the photocurrent was very stable throughout the course of the experiment. The small nonlinearities in the O_2 evolution data result from formation, accumulation, and release of oxygen bubbles at the photoanode surface. Overall, the data show an average O_2 evolution rate of ~2.4 × 10^{-9} mol/s·cm^2 with 1 sun illumination. The solid pink curve plots the O_2 concentration predicted from the photocurrent assuming 100% faradaic efficiency. The excellent agreement between this line and the experimental O_2 evolution data confirms that the photocurrent densities measured for this Co-Pi/W:$BiVO_4$ photoanode are associated with water oxidation and hence that Co-Pi substantially improves the solar water oxidation efficiency of W:$BiVO_4$.

C. Comparison with H_2O_2 Oxidation. The remarkable reduction in onset potential for PEC water oxidation by W:$BiVO_4$ photoanodes following Co-Pi deposition implies facile water oxidation under these experimental conditions. To assess the effectiveness of this catalyst, an easily oxidized surrogate substrate was sought that would reveal the ultimate performance limit for these photoanodes in the absence of surface electron−hole recombination. Various sacrificial reductants such as quinol[38] and Na_2SO_3[18] have been used for this purpose previously. Recently, PEC H_2O_2 oxidation was shown to provide a useful metric for assessing the performance limits of α-Fe_2O_3 photoanodes.[39] With a structure similar to that of H_2O, oxidation kinetics at least 10 times faster than that of H_2O, and a low reduction potential of 0.68 V compared to 1.23 V for H_2O, H_2O_2 is a suitable surrogate for H_2O, and we therefore examined PEC H_2O_2 oxidation by W:$BiVO_4$ photoanodes.

Figure 4 presents $J-V$ curves and photocurrent transients measured for a W:$BiVO_4$ photoanode with and without H_2O_2, and compares these data to parallel results collected during PEC water oxidation by the same photoanode following Co-Pi deposition, all in 0.1 M KPi buffer at pH 8. The onset potential for PEC water oxidation by the W:$BiVO_4$ photoanode is ~740 mV (Figure 4a). Spikes followed by slow decay are observed in the photocurrent transients at low potentials. These effects diminish with increasing applied potential, where the photocurrent responses become more square (Figure 4b,c). Together, these observations indicate the presence of surface recombination processes in which initial hole accumulation at the photoanode/electrolyte interface is followed by some degree of electron−hole recombination before steady-state photocurrents are reached. Recombination is most prevalent at low applied potentials, leading to little or no steady-state photocurrent. Adding 0.1 M H_2O_2 to the electrolyte suppresses these spikes, indicating suppressed surface recombination, and the onset potential shifts cathodically down to 290 mV. The square transient photocurrent responses seen in Figure 4b are consistent with the conclusion that all holes reaching the photoanode surface are successfully captured by H_2O_2. The PEC data collected with H_2O_2 as the surrogate substrate thus illustrate the limiting behavior that can be expected from these W:$BiVO_4$ photoanodes in the absence of surface recombination losses.

Figure 4 also plots results from PEC measurements performed after Co-Pi deposition onto W:$BiVO_4$, again collected in 0.1 M KPi at pH 8. The $J-V$ curve of the Co-Pi/W:$BiVO_4$ composite photoanode performing H_2O oxidation very closely resembles that of the W:$BiVO_4$ photoanode performing H_2O_2 oxidation. Very similar photocurrent densities are achieved for the two at all potentials below 1.5 V vs RHE, and their divergence above

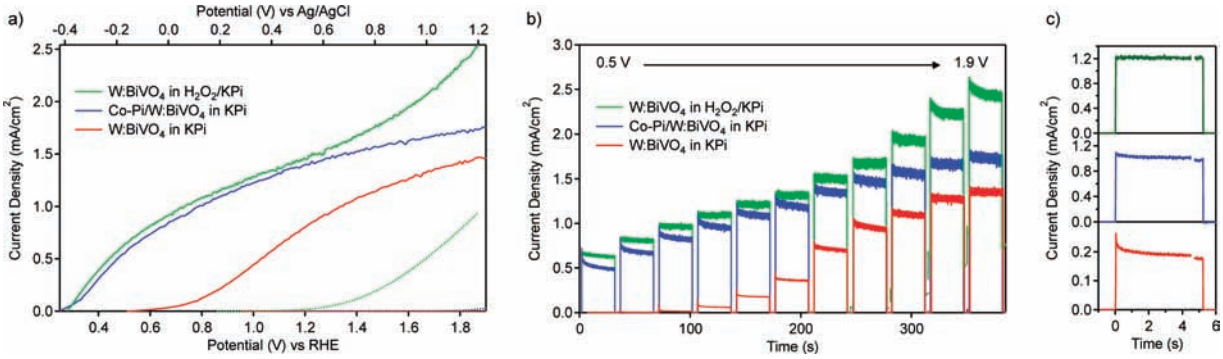

Figure 4. (a) $J-V$ curves measured for a W:$BiVO_4$ photoanode in 0.1 M KPi buffer (pH 8) under 1 sun AM 1.5 front-side illumination (solid) and in the dark (dotted). The red curve describes PEC water oxidation by the W:$BiVO_4$ photoanode, and the green curve describes the PEC behavior after addition of 0.1 M H_2O_2 to the electrolyte solution. The blue curve describes PEC water oxidation by the W:$BiVO_4$ photoanode after Co-Pi deposition. (b) Photocurrent transients associated with the curves in panel (a) as a function of increasing applied potentials (0.5, 0.6, 0.7, 0.8, 0.9, 1.0, 1.2, 1.4, 1.6, 1.8, and 1.9 V vs RHE). (c) Expanded view of the photocurrent transients measured at 0.9 V vs RHE, showing the first 4.5 s and the last 0.5 s of the 30 s pulse.

1.5 V vs RHE simply results from the large dark current for H_2O_2 oxidation at those potentials (Figure 4a, dotted). Like the curves obtained with H_2O_2 oxidation, the photocurrent transients observed from PEC water oxidation with the Co-Pi/W:$BiVO_4$ photoanode show nearly square profiles with only small initial peaks, most likely from cobalt oxidation. These results demonstrate that Co-Pi is highly effective at promoting water oxidation by W:$BiVO_4$ photoanodes, almost completely suppressing losses due to surface electron−hole recombination. Evidently, Co-Pi provides a facile route by which photogenerated holes in W:$BiVO_4$ can be captured and used in the productive four-electron oxidation of water. The similarity of the PEC responses for H_2O_2 oxidation with W:$BiVO_4$ and H_2O oxidation with Co-Pi/W:$BiVO_4$ further suggests that Co-Pi does not alter the characteristics of the photoanode/electrolyte interface, for example, by influencing charge separation within the space charge layer of the W:$BiVO_4$ electrode. Overall, these results show that Co-Pi makes W:$BiVO_4$ photoanodes as reactive toward H_2O as they are toward H_2O_2, a remarkable transformation.

■ ANALYSIS AND DISCUSSION

The productive and nonproductive kinetic processes relevant to PEC water oxidation by W:$BiVO_4$ and Co-Pi/W:$BiVO_4$ photoanodes are summarized in Figure 5. Here, J_{abs} is the photocurrent density that would result from an absorbed photon conversion efficiency (APCE) of 100%, that is, the photon absorption rate. Upon light absorption, part of J_{abs} is lost to bulk recombination, giving a charge-separation current density of $J_{sep} = J_{abs} - J_{br}$, where J_{br} describes bulk recombination, such that the quantum efficiency for migration of photogenerated holes to the semiconductor/electrolyte interface without being annihilated via bulk recombination is $\phi_{sep} = J_{sep}/J_{abs}$. For simplicity, we include recombination in the depletion region within J_{br}. This current density may then be reduced by surface recombination losses (J_{sr}) or be successfully converted to substrate oxidation (J_{ox}) such that the quantum efficiency for substrate oxidation by a surface hole is $\phi_{ox} = J_{ox}/J_{sep} = 1 - J_{sr}/J_{sep}$. When faradaic, the surviving electrons are collected at the back contact with the same rate as holes are converted to substrate oxidation, namely, with the observed PEC photocurrent density (J_{PEC}). The photocurrent density arising from PEC water oxidation is thus described by eq 1.

$$J_{PEC} = J_{abs}\phi_{sep}\phi_{ox} \quad (1)$$

The surface and bulk recombination processes in these W:$BiVO_4$ PEC cells can be assessed quantitatively by analysis of the data in Figure 4 using eq 1.[39] In the limit of rapid and facile substrate oxidation, such as with H_2O_2, surface recombination is completely suppressed and $\phi_{ox} = 1$. The photocurrent density in this limit is then $J_{PEC} \equiv J^{H_2O_2} = J_{abs}\phi_{sep}$. When probing H_2O oxidation with the same photoanode, $\phi_{ox} < 1$ and can be calculated from the ratio $J^{H_2O}/J^{H_2O_2}$. Similarly, ϕ_{sep} can be calculated from $J^{H_2O_2}/J_{abs}$. Here, $J_{abs} \sim 5.26$ mA/cm^2 is estimated from the absorption spectrum of the W:$BiVO_4$ photoanode used in Figure 4.

Figure 6 plots ϕ_{sep} and ϕ_{ox} determined in this way for W:$BiVO_4$ and Co-Pi/W:$BiVO_4$ photoanodes performing PEC water oxidation at various applied potentials. Before Co-Pi modification, ϕ_{ox} of the W:$BiVO_4$ photoanode is very low at potentials below 1.0 V vs RHE, but it increases to ~0.75 at 1.5 V vs RHE. After Co-Pi modification, ϕ_{ox} approaches unity throughout the entire potential range ($\phi_{ox} = 0.8-1.0$). Meanwhile, ϕ_{sep} increases gradually from ~0.1 to 0.3 over this potential range.

This analysis confirms the conclusion drawn above that Co-Pi almost completely suppresses surface recombination losses in W:$BiVO_4$ photoanodes. For bare W:$BiVO_4$ (Figure 5a), surface recombination (J_{sr}) is a major loss pathway and results in poor water oxidation (J_{ox}) and consequently poor PEC photocurrent densities, especially at low applied potentials. After Co-Pi modification, J_{ox} increases dramatically relative to J_{sr} such that ϕ_{ox} approaches unity (Figure 5b). Evidently, photogenerated holes that migrate to the W:$BiVO_4$ surfaces are captured by the Co-Pi electrocatalyst with near 100% quantum efficiency, where they also oxidize water with near 100% quantum efficiency. Overall, water oxidation becomes much more facile, making the desired catalysis kinetically competitive with nonproductive surface electron−hole recombination processes. It is not known whether this improvement stems from an absolute increase in J_{ox}, an absolute decrease in J_{sr}, or both.

Using ϕ_{sep} determined in the above analysis, the effective hole diffusion lengths (L_p) of W:$BiVO_4$ photoanodes can be estimated

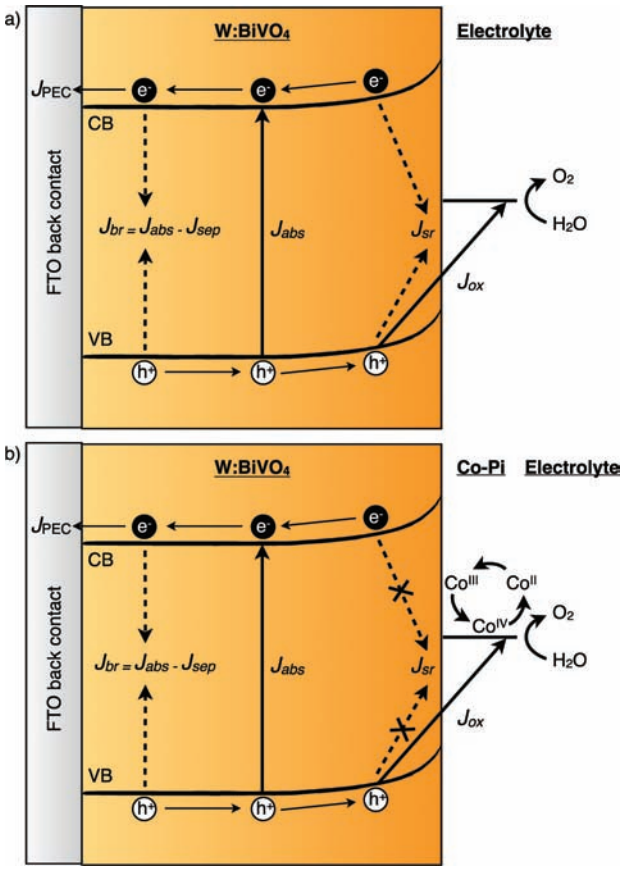

Figure 5. Energy diagram showing the kinetic processes active in the (a) W:$BiVO_4$ and (b) Co-Pi/W:$BiVO_4$ PEC photoanodes. Electron−hole pairs are generated with a current density associated with photon absorption (J_{abs}) and can recombine nonproductively with current densities associated with radiative or nonradiative bulk (J_{br}) and surface (J_{sr}) recombination. Electron collection at the back contact (J_{PEC}) and hole transfer to the oxidizable substrate (J_{ox}) are productive processes contributing to PEC device efficiency.

from the Gärtner model[40] using eq 2, where α is the absorption coefficient and W is the effective depletion layer width.[4,38,40]

$$\phi_{sep} = 1 - \frac{e^{-\alpha W}}{1 + \alpha L_p} \quad (2)$$

An absorption coefficient (α) of ~40 000 cm^{-1} at λ = 420 nm is estimated from the experimental absorption spectrum, and a dielectric constant of $\varepsilon_r \sim 68$ has been determined.[41,42] W at large bias (1.5 V) can be estimated from the Mott−Schottky analyses of various $BiVO_4$ and W:$BiVO_4$ photoanodes reported previously (see the Supporting Information for details).[11,15,18] Experimentally, $BiVO_4$ and W:$BiVO_4$ donor densities (N_d) from 10^{18} to 10^{21} cm^{-3} have been reported.[11,15,18] To ensure a reasonably general estimate of L_p, an even larger range ($N_d \sim 10^{18}-10^{23}$ cm^{-3}) was considered, but W is not strongly influenced by N_d at large bias. Using the above parameters, eq 2 yields a conservative general estimate of $L_p \sim 100-200$ nm (see the Supporting Information). Although ~10−100 times larger than that of α-Fe_2O_3, L_p in W:$BiVO_4$ is comparable to the absorption length (~250 nm at 420 nm) and hence still too small to not hinder performance, as illustrated by Figure 6.

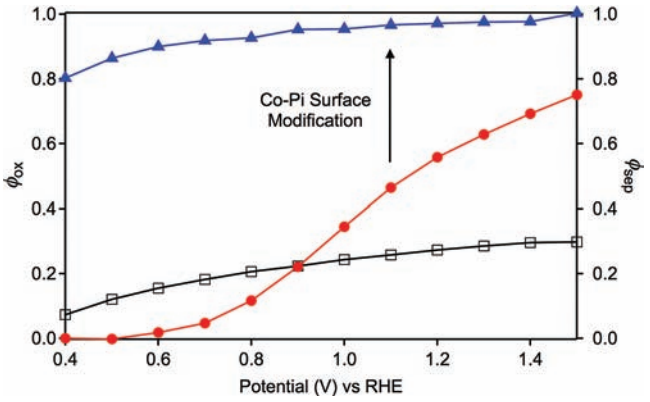

Figure 6. Substrate oxidation efficiencies (ϕ_{ox}) determined from the data in Figure 4 for Co-Pi/W:$BiVO_4$ (blue triangles) and W:$BiVO_4$ (red circles) photoanodes under PEC water oxidation conditions. The hollow squares plot the charge separation yields (ϕ_{sep}, applicable to both electrodes) at various potentials.

Importantly, this analysis allows the conclusion that PEC water oxidation by Co-Pi/W:$BiVO_4$ photoanodes is no longer limited by surface recombination effects, as was the case with W:$BiVO_4$ alone, but it is now limited solely by bulklike charge recombination processes (Figure 6). The latter could potentially be improved by use of thinner films (at the expense of J_{abs}), materials with higher structural quality and hence fewer bulk defects (e.g., epitaxial films), reduced dimensionality to accelerate charge collection (e.g., nanowires or mesostructures),[17,43−46] or via refined impurity doping. As proof of concept, the thicknesses of the W:$BiVO_4$ photoanodes described here (~300 nm) were optimized to give the highest photocurrent densities, but W:$BiVO_4$ films that were half as thick still gave ~80% of the same photocurrent density, suggesting significantly less bulk recombination in the thinner films.

Interestingly, the effect of Co-Pi surface modification is more substantial on W:$BiVO_4$ than observed previously on α-Fe_2O_3 photoanodes.[29,30] Surface recombination is a major loss mechanism in α-Fe_2O_3 photoanodes,[38,47] and in its absence (e.g., using H_2O_2) photocurrent onset potentials of ~0.5 V vs RHE have been achieved.[39] Surface catalysts including Co^{2+},[48] Co-Pi,[28−30] and IrO_2[49] all improve hole capture and conversion to water oxidation by mesostructured α-Fe_2O_3 photoanodes, but none have shown onset potentials below ~0.8 V vs RHE. Even with excellent surface catalysts, surface electron−hole recombination is thus still kinetically competitive in α-Fe_2O_3. Possible causes of this inefficiency include (i) incomplete surface coverage by the catalyst, perhaps due to the high porosity and surface roughness of the dendritic photoanodes, (ii) slow hole transfer from the surface to the catalyst, perhaps arising from the presence of deep hole traps,[38] or (iii) fast surface electron−hole recombination.[38,47] The latter two factors are most probable, and together they conspire to make surface electron−hole recombination in α-Fe_2O_3 photoanodes problematic even in the presence of effective surface electrocatalysts. In contrast, the data and analysis presented in Figures 4 and 6 indicate that surface electron−hole recombination has been largely eliminated in Co-Pi/W:$BiVO_4$ photoanodes.

Although characterized by an intense direct-gap absorption in the visible, the performance of $BiVO_4$ as a photoanode is limited by its inability to absorb more of the solar spectrum. From its 2.4−2.5 eV band gap, the maximum theoretical photocurrent

density achievable from $BiVO_4$ under 1 sun AM 1.5 sunlight is $J_{abs} \sim 6.5$ mA/cm^2. α-Fe_2O_3 (~2.1 eV) can reach roughly twice this theoretical maximum ($J_{abs} \sim 12.5$ mA/cm^2) under the same conditions, but its large bulk electron−hole recombination rates and short hole diffusion lengths limit ϕ_{sep} to ~0.25,[38,39] well below the values observed here for W:$BiVO_4$. Light harvesting by $BiVO_4$ could conceivably be improved through alloying, or this limitation could be circumvented by its integration with other materials in layered structures.[50]

Finally, we address the overall solar-to-hydrogen conversion efficiencies of PEC cells involving these Co-Pi/W:$BiVO_4$ composite photoanodes. Using the photocurrent from 1 sun AM 1.5 simulated solar irradiation (100 mW/cm^2), overall solar-to-hydrogen conversion efficiencies of the single-junction PEC process can be calculated from the Gibbs free energy of the reaction using eq 3, which accounts for the thermodynamic losses associated with application of an external anodic bias and assumes 100% faradaic efficiency.

$$\eta_{STH}\,(\%) = I\,(\mathrm{mA/cm^2}) \times (1.23\ \mathrm{V} - V_{app}) \qquad (3)$$

The maximum efficiency obtained from these Co-Pi/W:$BiVO_4$ composite photoanodes after accounting for external bias is 0.40% at 0.72 V vs RHE. This value is almost twice that of the best Co-Pi/α-Fe_2O_3 photoanodes reported previously (0.23%).[30] These numbers refer to the experimental solar power conversion efficiencies of these specific single-junction photoanodes. However, it is envisioned that PEC solar water splitting will not be implemented using single-junction devices with external bias, but instead the necessary anodic bias will be supplied by a second photoelectrode or PV device configured in a tandem geometry,[3,6,51,52] thereby improving η_{STH}. In this configuration, V_{app} is effectively zero and eq 3 becomes $\eta_{STH}\,(\%) = I\,(\mathrm{mA/cm^2}) \times 1.23$ V. Although both ϕ_{sep} and ϕ_{ox} are greater in W:$BiVO_4$ than in α-Fe_2O_3, Co-Pi/α-Fe_2O_3 photoanodes in this configuration provide larger solar-to-hydrogen conversion efficiencies (~4.1%) than Co-Pi/W:$BiVO_4$ photoanodes (1.7%), when calculated from photocurrents measured at 1.43 V vs RHE. This difference comes from the different light-harvesting abilities (J_{abs}) of the two materials. Practically, however, it is difficult to achieve the 1.43 V needed for this device structure without using two additional PV or PEC cells connected in series,[52] which raises costs. Co-Pi/W:$BiVO_4$ excels in the voltage range typically accessible from low-cost PEC or PV cells (<1.0 V), making it well suited for a simple tandem configuration.

CONCLUSION

Modification of W:$BiVO_4$ photoanode surfaces with the electrocatalyst Co-Pi has yielded an ~440 mV cathodic shift in the onset potential for PEC water oxidation. PEC experiments with H_2O_2 as a surrogate substrate have revealed that Co-Pi addition almost completely eliminates losses due to surface electron−hole recombination. The nearly quantitative substrate oxidation efficiencies (ϕ_{ox}) achieved with Co-Pi-modified W:$BiVO_4$ imply that photogenerated holes migrate to the W:$BiVO_4$ surfaces and are evidently captured by the Co-Pi electrocatalyst with nearly quantum efficiency, where they also oxidize water with nearly quantum efficiency. With Co-Pi, water oxidation becomes much more facile, making the desired catalysis outcompete unproductive surface electron−hole recombination.

The low absolute onset potential of ~310 mV vs RHE achieved at pH 8 with Co-Pi/W:$BiVO_4$ is promising for solar water splitting in low-cost tandem PEC cells. The results presented here demonstrate that Co-Pi largely eliminates a major performance limitation of W:$BiVO_4$ photoanodes by making J_{sr} kinetically uncompetitive with J_{ox}, even at the low applied potentials accessible from low-cost single-junction PEC or PV cells in a tandem device configuration. The primary performance limitation of the Co-Pi/W:$BiVO_4$ photoanodes is now their insufficient photon harvesting (J_{abs}), and efforts should be focused on developing this and related materials to improve this aspect.

ASSOCIATED CONTENT

Supporting Information. Additional characterization data including XRD, EDX, absorption, and PEC data, and details pertaining to L_p (7 figures, 1 table). This material is available free of charge via the Internet at http://pubs.acs.org.

AUTHOR INFORMATION

Corresponding Author
Gamelin@chem.washington.edu

ACKNOWLEDGMENT

This work was supported by the NSF (IGERT, DGE-050-4573), the University of Washington, and the UW Initiative Fund (UIF), and was partially conducted at the UW Nanotechnology User Facility, a member of NNIN. Initial stages of this research were supported by Sun Catalytix.

REFERENCES

(1) Fujishima, A.; Honda, K. *Nature* **1972**, *238*, 37.
(2) Bard, A. J.; Fox, M. A. *Acc. Chem. Res.* **1995**, *28*, 141.
(3) Grätzel, M. *Nature* **2001**, *414*, 338.
(4) Grimes, C. A.; Varghese, O. K.; Ranjan, S. *Light, Water, Hydrogen*; Springer: New York, 2007.
(5) Walter, M. G.; Warren, E. L.; McKone, J. R.; Boettcher, S. W.; Mi, Q.; Santori, E. A.; Lewis, N. S. *Chem. Rev.* **2010**, *110*, 6446.
(6) Alexander, B. D.; Kulesza, P. J.; Rutkowska, I.; Solarska, R.; Augustynski, J. *J. Mater. Chem.* **2008**, *18*, 2298.
(7) van de Krol, R.; Liang, Y.; Schoonman, J. *J. Mater. Chem.* **2008**, *18*, 2311.
(8) Scaife, D. E. *Sol. Energy* **1980**, *25*, 41.
(9) Kudo, A.; Ueda, K.; Kato, H.; Mikami, I. *Catal. Lett.* **1998**, *53*, 229.
(10) Tokunaga, S.; Kato, H.; Kudo, A. *Chem. Mater.* **2001**, *13*, 4624.
(11) Sayama, K.; Nomura, A.; Arai, T.; Sugita, T.; Abe, R.; Yanagida, S.; Oi, T.; Iwasaki, Y.; Abe, Y.; Sugihara, H. *J. Phys. Chem. B* **2006**, *110*, 11352.
(12) Yao, W.; Iwai, H.; Ye, J. *Dalton Trans.* **2008**, 1426.
(13) Luo, W.; Wang, Z.; Wan, L.; Li, Z.; Yu, T.; Zou, Z. *J. Phys. D: Appl. Phys.* **2010**, *43*, 405402.
(14) Ng, Y. H.; Iwase, A.; Kudo, A.; Amal, R. *J. Phys. Chem. Lett.* **2010**, *1*, 2607.
(15) Li, M.; Zhao, L.; Guo, L. *Int. J. Hydrogen Energy* **2010**, *35*, 7127.
(16) Sayama, K.; Wang, N.; Miseki, Y.; Kusama, H.; Onozawa-Komatsuzaki, N.; Sugihara, H. *Chem. Lett.* **2010**, *39*, 17.
(17) Su, J.; Guo, L.; Yoriya, S.; Grimes, C. A. *Cryst. Growth Des.* **2010**, *10*, 856.
(18) Ye, H.; Lee, J.; Jang, J. S.; Bard, A. J. *J. Phys. Chem. C* **2010**, *114*, 13322.
(19) Chatchai, P.; Kishioka, S.-y.; Murakami, Y.; Nosaka, A. Y.; Nosaka, Y. *Electrochim. Acta* **2010**, *55*, 592.
(20) Berglund, S. P.; Flaherty, D. W.; Hahn, N. T.; Bard, A. J.; Mullins, C. B. *J. Phys. Chem. C* **2011**, *115*, 3794.

(21) Hong, S. J.; Lee, S.; Jang, J. S.; Lee, J. S. *Energy Environ. Sci.* **2011**, *4*, 1781.
(22) Ye, H.; Park, H. S.; Bard, A. J. *J. Phys. Chem. C* **2011**, *115*, 12464.
(23) Yin, W.-J.; Wei, S.-H.; Al-Jassim, M. M.; Turner, J.; Yan, Y. *Phys. Rev. B: Condens. Matter Mater. Phys.* **2011**, *83*, 155102.
(24) Sun, J.; Zhong, D. K.; Gamelin, D. R. *Energy Environ. Sci.* **2010**, *3*, 1252.
(25) Kanan, M. W.; Nocera, D. G. *Science* **2008**, *321*, 1072.
(26) Lutterman, D. A.; Surendranath, Y.; Nocera, D. G. *J. Am. Chem. Soc.* **2009**, *131*, 3838.
(27) Surendranath, Y.; Kanan, M. W.; Nocera, D. G. *J. Am. Chem. Soc.* **2010**, *132*, 16501.
(28) Zhong, D. K.; Sun, J.; Inumaru, H.; Gamelin, D. R. *J. Am. Chem. Soc.* **2009**, *131*, 6086.
(29) Zhong, D. K.; Gamelin, D. R. *J. Am. Chem. Soc.* **2010**, *132*, 4202.
(30) Zhong, D. K.; Cornuz, M.; Sivula, K.; Grätzel, M.; Gamelin, D. R. *Energy Environ. Sci.* **2011**, *4*, 1759.
(31) Barroso, M.; Cowan, A. J.; Pendlebury, S. R.; Grätzel, M.; Klug, D. R.; Durrant, J. R. *J. Am. Chem. Soc.* **2011**, *133*, 14868.
(32) Steinmiller, E. M. P.; Choi, K.-S. *Proc. Natl. Acad. Sci. U.S.A.* **2009**, *106*, 20633.
(33) Seabold, J. A.; Choi, K.-S. *Chem. Mater.* **2011**, *23*, 1105.
(34) Young, E. R.; Costi, R.; Paydavosi, S.; Nocera, D. G.; Bulovic, V. *Energy Environ. Sci.* **2011**, *4*, 2058.
(35) Pijpers, J. J. H.; Winkler, M. T.; Surendranath, Y.; Buonassisi, T.; Nocera, D. G. *Proc. Natl. Acad. Sci. U.S.A.* **2011**, *108*, 10056.
(36) Sleight, A. W.; Aykan, K.; Rogers, D. B. *J. Solid State Chem.* **1975**, *13*, 231.
(37) Park, H. S.; Kweon, K. E.; Ye, H.; Paek, E.; Hwang, G. S.; Bard, A. J. *J. Phys. Chem. C* **2011**, *115*, 17870.
(38) Dare-Edwards, M. P.; Goodenough, J. B.; Hamnett, A.; Trevellick, P. R. *J. Chem. Soc., Faraday Trans.* **1983**, *79*, 2027.
(39) Dotan, H.; Sivula, K.; Grätzel, M.; Rothschild, A.; Warren, S. *Energy Environ. Sci.* **2011**, *4*, 958.
(40) Gärtner, W. W. *Phys. Rev.* **1959**, *116*, 84.
(41) Valent, M.; Suvorov, D. *J. Am. Ceram. Soc.* **2000**, *83*, 2721.
(42) Wee, S.-H.; Kim, D.-W.; Yoo, S.-I. *J. Am. Ceram. Soc.* **2004**, *87*, 871.
(43) Hagedorn, K.; Forgacs, C.; Collins, S.; Maldonado, S. *J. Phys. Chem. C* **2010**, *114*, 12010.
(44) Liu, R.; Lin, Y. J.; Chou, L. Y.; Sheehan, S. W.; He, W. S.; Zhang, F.; Hou, H. J. M.; Wang, D. W. *Angew. Chem., Int. Ed.* **2011**, *50*, 499.
(45) Lin, Y. J.; Zhou, S.; Sheehan, S. W.; Wang, D. W. *J. Am. Chem. Soc.* **2011**, *133*, 2398.
(46) Ling, Y. C.; Wang, G. M.; Wheeler, D. A.; Zhang, J. Z.; Li, Y. *Nano Lett.* **2011**, *11*, 2119.
(47) Klahr, B. M.; Martinson, A. B. F.; Hamann, T. W. *Langmuir* **2011**, *27*, 461.
(48) Kay, A.; Cesar, I.; Grätzel, M. *J. Am. Chem. Soc.* **2006**, *128*, 15714.
(49) Tilley, S. D.; Cornuz, M.; Sivula, K.; Grätzel, M. *Angew. Chem., Int. Ed.* **2010**, *49*, 6405.
(50) Sivula, K.; Formal, F. L.; Grätzel, M. *Chem. Mater.* **2009**, *21*, 2862.
(51) Arakawa, H.; Shiraishi, C.; Tatemoto, M.; Kishida, H.; Usui, D.; Suma, A.; Takamisawa, A.; Yamaguchi, T. *Proc. SPIE* **2007**, *6650*, 665003.
(52) Brillet, J.; Cornuz, M.; Le Formal, F.; Yum, J.-H.; Grätzel, M.; Sivula, K. *J. Mater. Res.* **2010**, *25*, 17.